Spectral Gap Extrapolation and Radio Frequency Interference Suppression Using 1D UNets

Arun Asokan Nair,* Akshay Rangamani,† Lam H. Nguyen,‡ Muyinatu A. Lediju Bell* and Trac D. Tran*
*Department of Electrical and Computer Engineering, Johns Hopkins University, Baltimore, MD
†Center for Brains, Minds and Machines, Massachusetts Institute of Technology, Boston, MA
‡RF Signal Processing and Modeling Branch, DEVCOM Army Research Laboratory, Adelphi, MD

2021 IEEE Radar Conference (RadarConf21) | 978-1-7281-7609-3/20/$31.00 ©2021 IEEE | DOI: 10.1109/RadarConf2147009.2021.9455241

***Abstract*—Modern ultra-wideband (UWB) radar systems transmit a wide range of frequencies, spanning hundreds of MHz to a few GHz, to achieve improved penetration depth and narrower pulse width. A common challenge faced is the presence of other commercial transmission equipment operating in the same band, causing radio frequency interference (RFI). To overcome this RFI issue, radar systems have been developed to either avoid operating in bands with RFI or suppress the RFI after reception. In this work, we examine both families of operation and demonstrate that 1D convolutional neural networks based on the UNet architecture can provide powerful signal enhancement capabilities on raw UWB radar data. The model is *trained purely on simulated data* and translated to real UWB data, achieving impressive results compared to traditional sparse-recovery baseline algorithms.**

***Index Terms*—Spectral gap extrapolation, radio frequency interference suppression, ultra-wideband radar, convolutional neural network**

I. Introduction

Ultra-wideband (UWB) radar systems have gained significant traction due to their superior penetration capability and improved imaging resolution [1]. The U.S. Army, for example, has been developing UWB radar systems for detection of difficult targets in foliage penetration [2], ground penetration [3], and sensing-through-the-wall [4]. For superior penetration ability, these systems must operate in the low-frequency spectrum that spans from under 100 MHz to several GHz.

As well as requiring low frequency operation for penetration, synthetic aperture radar (SAR) obtains high resolution images by transmitting pulses with UWB — the wider the pulse bandwidth in frequency, the narrower the pulse in time, improving spatial resolution [1], [5], [6]. However, the transmission of UWB pulses is often complicated by the presence of other communication equipment sharing the same spectrum. UWB radar signals span a wide spectrum that also includes radio, TV, cellular phones, and other communication systems, each of which inject radio frequency interference (RFI) into the data.

This leaves the radar system with two approaches to solve the problem. The first is to continue to transmit in those bands and denoise the RFI-contaminated radar data after reception [7], [8]. The second is to employ stepped-frequency radars (SFRs) [9]–[11] with frequency hopping capabilities. SRFs allow for the transmission of UWB pulses while still maintaining precise control over the transmitted spectrum, utilizing frequency synthesizers that can be configured to avoid transmitting energy in prohibited/interference frequency bands. Unfortunately, notches in the frequency domain caused by this transmission method create strong sidelobes (or ringing artifacts) in the received time domain data, which requires further signal processing to ameliorate.

One could argue that the second approach (spectral gap extrapolation) partially subsumes the first approach (RFI suppression) — as one can always suppress frequency components where there is heavy RFI by setting those Fourier coefficients to zero and then proceeding to extrapolate the resultant spectral gaps. However, this line of thinking has two major problems. First, it is assumes that the operating spectrum affected by RFI is known exactly, or else unnecessary performance degradation will be introduced. Second, there are often better performing pre-processing methods than notching RFI-affected radar data. Thus, it is better to deal with each scenario separately.

Sparsity-based signal processing methods have achieved great success in both suppressing RFI [12], [13] and performing spectral gap extrapolation [14]–[16] to combat frequency notches. However, they still struggle to distinguish neighboring and/or weak targets at fine resolution and performance drops precipitously when the RFI bands (or notches) are wider or affect more frequencies.

Deep neural networks (DNNs), and deep convolutional neural networks (CNNs) in particular, have recently become immensely popular for a wide variety of traditional signal processing tasks like image segmentation [17], denoising [18], and point source localization in the presence of noise [19], displaying extremely impressive results. In the radar domain, DNNs have been successfully used for target detection and classification [20], antenna selection in cognitive radar [21], interference mitigation [22] and vehicle detection [23] in automotive applications, and activity recognition [24]–[26] applications in indoor monitoring. For SAR specifically, image despeckling [27], phase error correction [28], change detection [29], ship detection [30] and discrimination [31], and image reconstruction [32], [33] are just some of the problems where deep learning has helped.

Past work from our group [34], [35] investigated the use of a specific kind of deep neural network, called a generative adversarial network (GAN) [36], to perform spectral gap

extrapolation and obtained promising results. In this work, we expand upon the prior work in three important ways. First, in addition to spectral gap extrapolation, we also demonstrate successful RFI suppression using a deep network. Second, we demonstrate state-of-the-art results on real UWB SAR data. Third, we demonstrate this success via a simple 1D CNN based on the UNet [17] architecture, which is easier and more stable to train than a GAN.

II. Method

The goal of this work is to successfully recover clean raw UWB SAR data, $\mathbf{x}$, from noisy observations, $\mathbf{y}$, observed by sensors. Specifically, we consider three kinds of noise: *(i)* RFI, where the majority of the energy of the interfering signal is located in a few frequency bands; *(ii)* random spectral gaps, where several randomly chosen narrow spectral bands are missing; and *(iii)* a block spectral gap, where a single contiguous segment of the operating spectrum is missing. We investigate the efficacy of using 1D UNet [17] CNNs to remove each kind of noise – *a different 1D UNet is trained for each noise type* – and compare it with competitive baselines. The UNet is trained end-to-end (i.e., all layers are learned simultaneously).

A. Ground-truth Dataset for Network Training

To create the clean training data, a sparsity-based linear model widely employed in compressed sensing SAR [16] was used. The scene of interest was modeled as a sparse collection of independent point scatterers randomly distributed in space. As the model is linear, it is assumed that the scatterers do not interact with each other, and the final received signal is simply the sum of reflections from each of the individual scatterers. Mathematically, the model can be expressed as

$$x(t) = \sum_i r(z_i) p(t; z_i) \tag{1}$$

where $x(t)$ is the received raw SAR signal, $r(z_i)$ is the reflectivity of a point scatterer located at z_i, and $p(t; z_i)$ represents the point spread function of a scatterer with unit reflectivity located at z_i.

To implement (1), the template pulse $p(t; 0)$ is linearly shifted to represent the response from various locations $p(t; z)$, and the shifted pulses are stored as columns of a dictionary $\mathbf{P}$. Simulating data comes down to sampling possible sparse code coefficients, $\mathbf{r}$, to combine with the dictionary to yield the received raw data

$$\mathbf{x} = \mathbf{P}\mathbf{r}. \tag{2}$$

An advantage of this modeling approach over [35] is that we operate on the received 1D data from each aperture element individually, i.e., the geometry of the entire aperture does not matter — a neural network trained on one geometry can generalize to another. The actual image creation (slow-time processing) is accomplished later.

The template pulse is sampled at 37.48 GHz and contains most of its energy, as measured by the -12 dB points, between 380 and 2080 MHz. We set the signal dimension (i.e., the lengths of $\mathbf{x}$ and $\mathbf{r}$) to a fixed value of 1024 samples.

A total of 1,000,000 possible sparse codes were sampled from realistic sparse code distributions mimicking coefficients obtained in side-looking SAR to construct the ground-truth training dataset. An additional 12,500 samples (of course, with no intersection with the training set) were generated and reserved as a clean simulated test set. Lastly, 3,600 samples corresponding to two real data acquisitions of 1,800 samples each from circular-sensing SAR were reserved as a clean real test set. Each of these were then corrupted with noise to generate paired clean+noisy data, as detailed in Section II-B.

B. Noise Modeling

In this work, we focus on three kinds of noise – RFI, random spectral gaps, and a block spectral gap. Below, we provide details on each and elaborate on their modeling.

1) Radio Frequency Interference: The scenario of RFI occurs when an interfering source transmits most of its energy in a small subset of the spectrum of the UWB SAR. Mathematically, this can be modeled as an additive noise:

$$\mathbf{y}_{int} = \mathbf{x} + \mathbf{i} \tag{3}$$

where $\mathbf{i}$ is the RFI signal and $\mathbf{y}_{int}$ represents the observed noisy data.

The RFI, $\mathbf{i}$, used in this work is obtained from real RFI data recorded over a long time horizon. We split the recorded RFI signal into two parts — we use samples from the first half to generate training data and samples from the second half to generate test data. For each set, we mix a randomly chosen clean signal and RFI samples at various signal-to-noise ratios (SNRs) randomly chosen from -15, -10, -5, 0, 5, and 10 dB.

2) Random Spectral Gaps: The scenario of random spectral gaps occurs when several narrowband sections of the radar spectrum might be restricted and off-limits to data transmission. Mathematically, this can be modeled as a masking operation in the Fourier domain:

$$FFT(\mathbf{y}_{rg}) = \mathbf{m}_{rg} \odot FFT(\mathbf{x}) \tag{4}$$

where $\mathbf{m}_{rg}$ is a binary mask. The total signal bandwidth is divided into 10 narrow spectral bands and depending on the missing percentage, several bands are masked to zero, while the mask affecting the remaining coefficients is one. Here, $\mathbf{y}_{rg}$ represents the observed noisy data suffering from random spectral gaps.

Noisy data corresponding to spectral missing percentages of 50%, 60%, 70%, 80%, and 90% were generated for use in training and testing by randomly choosing and eliminating the chosen percentage of spectral coefficients from the ground-truth data.

3) Block Spectral Gap: The scenario of a centered block spectral gap occurs as the worst-case scenario when a contiguous section of the radar spectrum centered on the middle of the transmitted template pulse's bandwidth (where most of the pulse's energy is located) is marked as restricted and

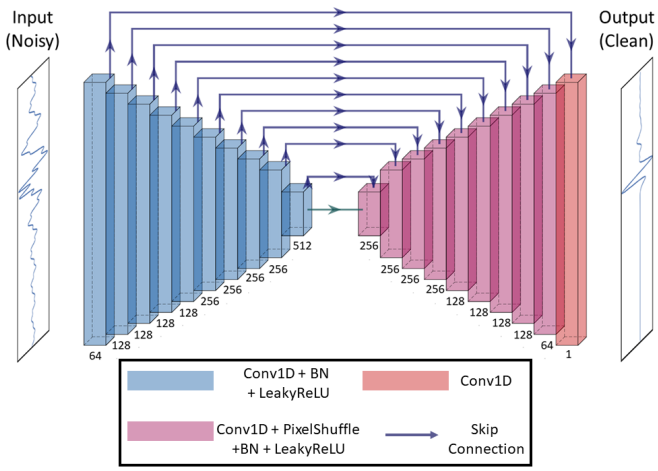

Fig. 1. Proposed 1D UNet for UWB signal denoising. Noisy input data degraded by one of RFI, random spectral gaps, or a centered block spectral gap is denoised by the network trained on that noise type to yield an estimate of the clean target signal.

not allowed for transmission. Mathematically, this too can be modeled as a masking operation in the Fourier domain:

$$FFT(\mathbf{y}_{bg}) = \mathbf{m}_{bg} \odot FFT(\mathbf{x}) \tag{5}$$

where $\mathbf{m}_{bg}$ is a binary mask of zeros and ones determining which spectral coefficients are transmitted and which are not available. Unlike $\mathbf{m}_{rg}$ where the zeros are chosen to lie randomly in several narrow spectral gaps, in $\mathbf{m}_{bg}$ the vanishing region is located contiguously around the center frequency of the pulse. We use $\mathbf{y}_{bg}$ to represent the observed noisy data suffering from the centered block spectral gap.

Noisy data corresponding to spectral missing percentages of 50%, 60%, 70%, 80%, and 90% were generated for use in training and testing by setting to zero the chosen percentage of spectral coefficients of the clean data.

C. Neural Network Details

The network architecture used in this study is an adaptation of the popular UNet [17] architecture adapted to the 1D signal processing scenario. A visualization of its structure with the number of filters in each layer is presented in Fig. 1. It has a fully convolutional encoder-decoder type architecture, with a total of 20 layers – 10 layers each in the encoder and decoder. Convolutional kernel size is set to 5, with encoder layers having a stride of 2 to downsample the feature map in each layer (except for the input layer, which has a stride of 1). The decoder layers all have a stride of 2 to upsample the feature map at each layer. Skip connections are employed to connect encoder and decoder layers at the same level. Each layer uses BatchNorm (BN) [37] and LeakyReLU as its nonlinearity components (except for the output layer, which has neither). Sub-pixel convolutions, also known as PixelShuffle [38], [39], are used in the decoder as they seem to work better than transposed convolutions and they reduce recovery artifacts. The total number of trainable parameters in the network is 7,182,209.

A different network was trained for each noise type, but in each case, a single network was trained to denoise all noise conditions for the chosen noise type. All networks were trained with *L1Loss*, or mean absolute error, as the loss criterion, using the Adam optimizer [40] with a batch size of 64 and a learning rate of 0.0001.

D. Baselines

For RFI suppression, we implement a simple but effective frequency masking baseline. As most of the energy of the bandlimited RFI signal was observed to be between 256 and 476 MHz, the Fourier coefficients of the noisy input data between those limits were set to zero to yield a baseline enhanced signal with which to compare our neural network approach.

For spectral gap extrapolation on signals with random spectral gaps, we implement a sparse coding baseline via Orthogonal Matching Pursuit (OMP) [41] (or any of its variants such as [42]), following the approach proposed in [15], [16]. Similar to the way the dictionary $\mathbf{P}$ in (2) was constructed, a dictionary $\tilde{\mathbf{P}}$ was constructed by linearly shifting a corrupted transmitted pulse (possessing the same random spectral gap structure as the noisy data). Every random spectral gap structure encountered required its own tailored dictionary. Sparse coding was performed on the noisy input data using this corrupted dictionary. Assuming robust sparse codes, we obtained the recovered signal from the clean dictionary $\mathbf{P}$. The number of sparse coefficients in the OMP algorithm, K, was tuned on the test data itself. While this is not possible in practice, it does yield the best possible performance for the baseline algorithm.

For spectral gap extraction on signals with a centered contiguous gap, a sparse coding baseline very similar to the one implemented for the random spectral gaps was used. Here, since the gap structure remains the same for all data at a specific missing percentage, the corrupted dictionary with linearly shifted corrupted template pulses $\overline{\mathbf{P}}$ could be shared. Sparse coding was performed on the noisy input data using this corrupted dictionary, and the sparse code thus obtained was combined with the clean dictionary $\mathbf{P}$ to yield the baseline enhanced signal. Again, we manually tune the OMP hyperparameter, K, tuned on the test data itself to obtain the best performance for comparison.

E. Evaluation

Quantitative evaluation of denoising performance is carried out with the general purpose SNR metric reported in the dB scale. It was measured as

$$\text{SNR}(\mathbf{x}, \mathbf{z}) = 20 \log_{10} \frac{||\mathbf{x}||_2}{||\mathbf{x} - \mathbf{z}||_2} \tag{6}$$

where $\mathbf{x}$ is the target clean signal, $\mathbf{z}$ is the signal being compared to it, and $||.||_2$ is the ℓ_2 norm.

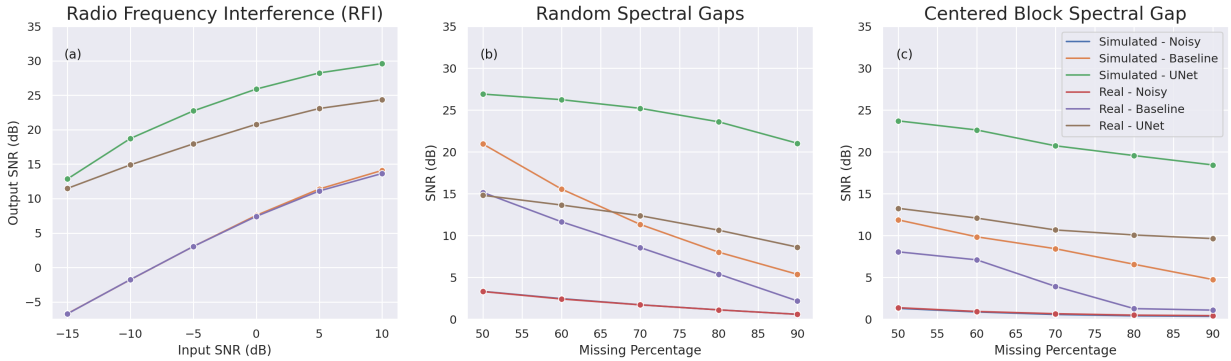

Fig. 2. Data quality (measured by SNR in dB) for simulated and real noisy, baseline enhanced, and UNet enhanced data for (a) RFI affected data as a function of input SNR, (b) random spectral gaps affected data as a function of missing percentage, and (c) a centered block spectral gap affected data as a function of missing percentage. Best viewed in color.

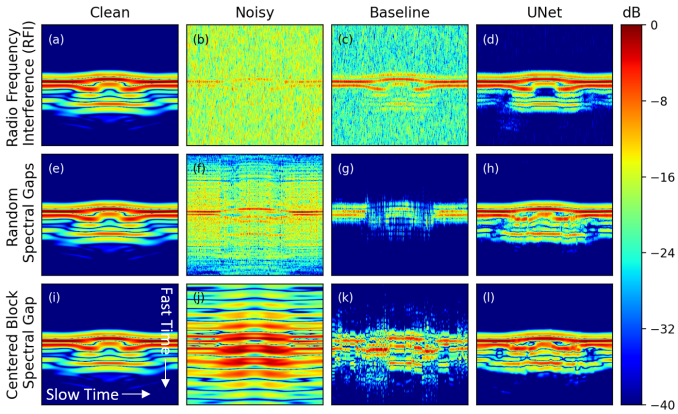

Fig. 3. Visualization of real data denoising under challenging noise conditions. (a), (e), and (i), are each the clean target data. (b) Noisy data suffering from RFI with an SNR of -15 dB, (f) noisy data suffering from random spectral gaps with a spectral missing percentage of 90%, and (j) noisy data suffering from a centered block spectral gap with a spectral missing percentage of 90%. (c), (g), and (k) are the enhanced outputs from each of the baseline methods. (d), (h), and (l) are the enhanced outputs from each of the UNets trained to tackle a specific noise type.

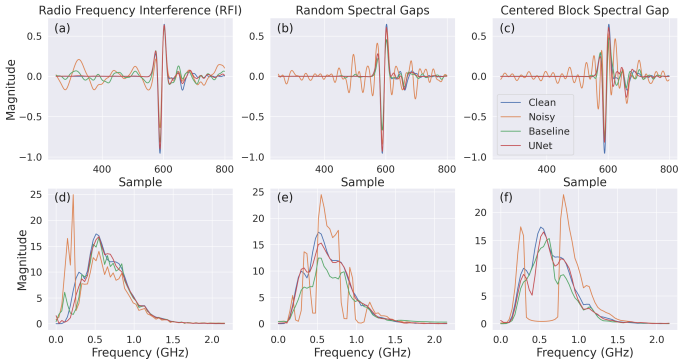

Fig. 4. Visualization of real data denoising under challenging noise conditions for a single aperture element. A single representative aperture element is chosen from Fig. 3 and the radar waveforms corresponding to clean, noisy, baseline enhanced, and UNet enhanced data are plotted for RFI, random spectral gaps, and a centered block spectral gap, in (a), (b), and (c), respectively, with plots of the corresponding magnitude spectra in (d), (e), and (f), respectively. Best viewed in color.

III. Experiments

A. Radio Frequency Interference

Fig. 2(a) shows quantitative comparisons between the output SNR (in dB) of the UNet-based approach and the baseline approach that sets the Fourier coefficients affected strongly by RFI to zero for various input SNR values. It is observed that the UNet approach consistently outperforms the baseline on both the simulated and real test data for all input SNR values, delivering an average SNR gain (averaged over all input SNR values) of 25.5 and 21.87 dB on simulated and real data, respectively. In contrast, the baseline only yields an average simulated and real SNR gain of 7.1 and 7.0 dB, respectively.

To visualize these results, Fig. 3 (top row) shows (from left to right) (a) clean target data, (b) noisy input data corrupted by RFI, (c) baseline enhanced output data, and (d) enhanced output data obtained from the UNet. All images are plotted with a dynamic range of 40 dB. The specific example displayed here is the real test data in the most challenging scenario when RFI is very strong (input SNR is -15dB). As a result, the target structure is barely visible in the noisy input data shown in Fig. 3(b). The baseline algorithm enhances the image slightly, but the UNet does significantly better, efficiently exploiting the structure in the RFI signal and suppressing it.

We study the enhancement in more detail by plotting the 1D radar waveforms received by a single representative aperture element from Fig. 3 in Fig. 4(a). It is clear here too that the UNet does a better job suppressing the RFI and recovering the shape of the target pulse. This is confirmed again when examining the corresponding magnitude spectra in Fig. 4(d).

Figs. 5 and 6 contain similar RFI denoising results for the second real dataset under milder noise.

B. Random Spectral Gaps

Fig. 2(b) plots the SNRs (in dB) versus the missing spectrum percentage for noisy input affected by random spectral gaps, baseline enhanced output, and UNet enhanced output,

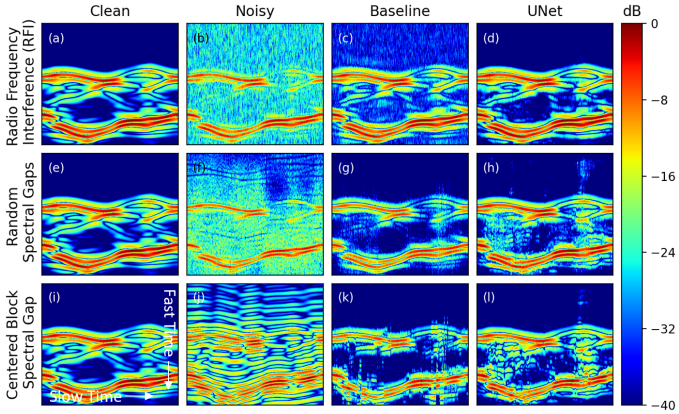

Fig. 5. (top) Visualization of real data denoising under milder noise conditions. (a), (e), and (i), are each the clean target data. (b) Noisy data suffering from RFI with an SNR of 0 dB, (f) noisy data suffering from random spectral gaps with a spectral missing percentage of 50%, and (j) noisy data suffering from a centered block spectral gap with a spectral missing percentage of 50%. (c), (g), and (k) are the enhanced outputs from each of the baseline methods. (d), (h), and (l) are the enhanced outputs from each of the UNets trained to tackle a specific noise type.

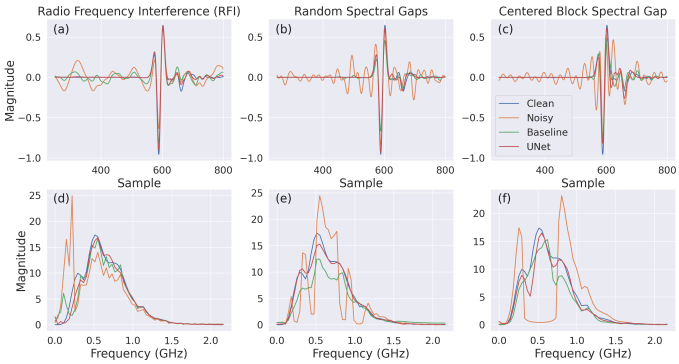

Fig. 6. Visualization of real data denoising under milder noise conditions for a single aperture element. A single representative aperture element is chosen from Fig. 5 and the radar waveforms corresponding to clean, noisy, baseline enhanced, and UNet enhanced data are plotted for RFI, random spectral gaps, and a centered block spectral gap, in (a), (b), and (c), respectively, with plots of the corresponding magnitude spectra in (d), (e), and (f), respectively. Best viewed in color.

on both simulated and real test data. The UNet approach consistently performs as well as or better than the baseline on both simulated and real test data for all input SNR values, delivering an average SNR gain (averaged over all input SNR values) of 22.75 and 10.19 dB on simulated and real data, respectively. In contrast, the baseline only yields an average simulated and real SNR gain of 10.40 and 6.76 dB, respectively.

The network output SNR here on real data is lower than the case of RFI because we train our networks on simulated data and there is a domain shift between the training data and test data that negatively impacts network performance, which is especially impactful when the noise is signal-dependent like random spectral gaps. Thus, it is important to make our training data as representative of real test data as possible. This is the major current bottleneck to further improvements within this framework.

Fig. 3 (middle row) shows (from left to right) (e) clean target data, (f) noisy input data corrupted by random spectral gaps setting 90% of the spectrum to zero, (g) enhanced output data obtained from the OMP baseline, and (h) enhanced output data obtained from the UNet. The UNet does well in recovering the target clean data, outperforming the baseline in this severe noise condition and recovering the target structures. The radar signals recorded by a single representative aperture and its magnitude spectra can be observed in Fig. 4(b) and (e), respectively.

Figs. 5 and 6 contain similar random spectral gap extrapolation results for the second real dataset under milder noise.

C. Centered Block Spectral Gap

Fig. 2(c) plots SNR (in dB) versus missing spectrum percentage for noisy input data affected by a centered block spectral gap, baseline enhanced output, and UNet enhanced output, on both simulated and real test data. The UNet-based approach outperforms the baseline OMP approach on all missing percentages on both simulated and real data, yielding a SNR gain of 20.31 and 10.37 dB, respectively, compared to 7.60 and 3.51 dB, respectively. The network output SNR here on real data though is lower than the case of RFI due to the same data domain shift as elaborated on in Section III-B.

Fig. 3 (bottom row) shows (from left to right) (i) clean target data, (j) noisy input data corrupted by a centered block spectral gap setting 90% of the spectrum to zero, (k) enhanced output data obtained from the OMP baseline, and (l) enhanced output data obtained from the UNet. The UNet does well, largely eliminating ringing artifacts and recovering target structural information better than OMP. This observation is confirmed by studying closely the radar signals recorded by a single representative aperture and its magnitude spectra in Fig. 4(c) and (f), respectively.

Figs. 5 and 6 contain similar block spectral gap extrapolation results for the second real dataset under milder noise.

IV. Conclusion

In this work, we demonstrated the efficacy of using 1D UNet networks to address three types of noise widely encountered by a UWB SAR – bandlimited RFI, random spectral gaps, and a contiguous block spectral gap, with the networks – one trained for each noise type – achieving good results even in challenging scenarios and displaying the recovery robustness at multiple noise levels. We trained our model purely on simulated data generated by a simple sparse linear model and demonstrated the network's remarkable generalization to real test data. Since our approach operates on individual data apertures, one key benefit is that the test sensor geometry is no longer required to match the training sensor geometry. In other words, our approach is less scene-dependent. In fact, we trained our networks using synthetically generated data on a side-looking geometry and successfully tested our networks on raw SAR data collected from a circular 360°-sensing geometry.

REFERENCES

[1] James D Taylor, *Ultrawideband radar: applications and design*, CRC Press, 2012.

[2] Lam H Nguyen, Ravinder Kapoor, and Jeffrey Sichina, "Detection algorithms for ultrawideband foliage-penetration radar," in *Radar Sensor Technology II*. International Society for Optics and Photonics, 1997, vol. 3066, pp. 165–176.

[3] Lam H Nguyen, Karl A Kappra, David C Wong, Ravinder Kapoor, and Jeffrey Sichina, "Mine field detection algorithm utilizing data from an ultrawideband wide-area surveillance radar," in *Detection and Remediation Technologies for Mines and Minelike Targets III*. International Society for Optics and Photonics, 1998, vol. 3392, pp. 627–643.

[4] Lam Nguyen, Marc Ressler, and Jeffrey Sichina, "Sensing through the wall imaging using the army research lab ultra-wideband synchronous impulse reconstruction (uwb sire) radar," in *Radar Sensor Technology XII*. International Society for Optics and Photonics, 2008, vol. 6947, p. 69470B.

[5] Lawrence Carin, Norbert Geng, Mark McClure, Jeffrey Sichina, and Lam Nguyen, "Ultra-wide-band synthetic-aperture radar for mine-field detection," *IEEE Antennas and Propagation Magazine*, vol. 41, no. 1, pp. 18–33, 1999.

[6] Mehrdad Soumekh, *Synthetic aperture radar signal processing*, vol. 7, New York: Wiley, 1999.

[7] Timothy Miller, Lee Potter, and John McCorkle, "Rfi suppression for ultra wideband radar," *IEEE transactions on aerospace and electronic systems*, vol. 33, no. 4, pp. 1142–1156, 1997.

[8] Lam H Nguyen and Trac D Tran, "Estimation and extraction of radio-frequency interference from ultra-wideband radar signals," in *2015 IEEE International Geoscience and Remote Sensing Symposium (IGARSS)*. IEEE, 2015, pp. 2848–2851.

[9] Cam Nguyen and Joongsuk Park, *Stepped-Frequency Radar Sensors: Theory, Analysis and Design*, Springer, 2016.

[10] Brian R Phelan et al., "Design of ultrawideband stepped-frequency radar for imaging of obscured targets," *IEEE Sensors Journal*, vol. 17, no. 14, pp. 4435–4446, 2017.

[11] Brian R Phelan et al., "System upgrades and performance evaluation of the spectrally agile, frequency incrementing reconfigurable (safire) radar system," in *Radar Sensor Technology XXI*. International Society for Optics and Photonics, 2017, vol. 10188, p. 1018812.

[12] Lam H Nguyen and Trac D Tran, "Rfi-radar signal separation via simultaneous low-rank and sparse recovery," in *2016 IEEE Radar Conference (RadarConf)*. IEEE, 2016, pp. 1–5.

[13] Yongping Song, Jun Hu, Yongpeng Dai, Tian Jin, and Zhimin Zhou, "Estimation and mitigation of time-variant rfi in low-frequency ultra-wideband radar," *IEEE Geoscience and Remote Sensing Letters*, vol. 15, no. 3, pp. 409–413, 2018.

[14] Mujdat Cetin and Randolph L Moses, "Sar imaging from partial-aperture data with frequency-band omissions," in *Algorithms for Synthetic Aperture Radar Imagery XII*. International Society for Optics and Photonics, 2005, vol. 5808, pp. 32–43.

[15] Lam Nguyen and Thong Do, "Recovery of missing spectral information in ultra-wideband synthetic aperture radar (sar) data," in *2012 IEEE Radar Conference*. IEEE, 2012, pp. 0253–0256.

[16] Lam H Nguyen, Trac Tran, and Thong Do, "Sparse models and sparse recovery for ultra-wideband sar applications," *IEEE Transactions on Aerospace and Electronic Systems*, vol. 50, no. 2, pp. 940–958, 2014.

[17] Olaf Ronneberger, Philipp Fischer, and Thomas Brox, "U-net: Convolutional networks for biomedical image segmentation," in *International Conference on Medical Image Computing and Computer-Assisted Intervention*. Springer, 2015, pp. 234–241.

[18] Kai Zhang, Wangmeng Zuo, Yunjin Chen, Deyu Meng, and Lei Zhang, "Beyond a gaussian denoiser: Residual learning of deep cnn for image denoising," *IEEE Transactions on Image Processing*, vol. 26, no. 7, pp. 3142–3155, 2017.

[19] Derek Allman, Austin Reiter, and Muyinatu A Lediju Bell, "Photoacoustic source detection and reflection artifact removal enabled by deep learning," *IEEE Transactions on Medical Imaging*, vol. 37, no. 6, pp. 1464–1477, 2018.

[20] Daniel Brodeski, Igal Bilik, and Raja Giryes, "Deep radar detector," in *2019 IEEE Radar Conference (RadarConf)*. IEEE, 2019, pp. 1–6.

[21] Ahmet M Elbir, Kumar Vijay Mishra, and Yonina C Eldar, "Cognitive radar antenna selection via deep learning," *IET Radar, Sonar & Navigation*, vol. 13, no. 6, pp. 871–880, 2019.

[22] Jiwoo Mun, Heasung Kim, and Jungwoo Lee, "A deep learning approach for automotive radar interference mitigation," in *2018 IEEE 88th Vehicular Technology Conference (VTC-Fall)*. IEEE, 2018, pp. 1–5.

[23] Bence et al. Major, "Vehicle detection with automotive radar using deep learning on range-azimuth-doppler tensors," in *Proceedings of the IEEE International Conference on Computer Vision Workshops*, 2019, pp. 0–0.

[24] Sevgi Zubeyde Gurbuz and Moeness G Amin, "Radar-based human-motion recognition with deep learning: Promising applications for indoor monitoring," *IEEE Signal Processing Magazine*, vol. 36, no. 4, pp. 16–28, 2019.

[25] Branka Jokanovic, Moeness Amin, and Fauzia Ahmad, "Radar fall motion detection using deep learning," in *2016 IEEE Radar Conference (RadarConf)*. IEEE, 2016, pp. 1–6.

[26] Mehmet Saygın Seyfioğlu, Ahmet Murat Özbayoğlu, and Sevgi Zubeyde Gürbüz, "Deep convolutional autoencoder for radar-based classification of similar aided and unaided human activities," *IEEE Transactions on Aerospace and Electronic Systems*, vol. 54, no. 4, pp. 1709–1723, 2018.

[27] Gang Zhang, Zhi Li, Xuewei Li, and Yiqiao Xu, "Learning synthetic aperture radar image despeckling without clean data," *Journal of Applied Remote Sensing*, vol. 14, no. 2, pp. 026518, 2020.

[28] Eric Mason, Bariscan Yonel, and Birsen Yazici, "Deep learning for radar," in *2017 IEEE Radar Conference (RadarConf)*. IEEE, 2017, pp. 1703–1708.

[29] Maoguo Gong, Jiaojiao Zhao, Jia Liu, Qiguang Miao, and Licheng Jiao, "Change detection in synthetic aperture radar images based on deep neural networks," *IEEE transactions on neural networks and learning systems*, vol. 27, no. 1, pp. 125–138, 2015.

[30] Zhipeng Deng, Hao Sun, Shilin Zhou, and Juanping Zhao, "Learning deep ship detector in sar images from scratch," *IEEE Transactions on Geoscience and Remote Sensing*, vol. 57, no. 6, pp. 4021–4039, 2019.

[31] Colin P Schwegmann, Waldo Kleynhans, Brian P Salmon, Lizwe W Mdakane, and Rory GV Meyer, "Very deep learning for ship discrimination in synthetic aperture radar imagery," in *2016 IEEE International Geoscience and Remote Sensing Symposium (IGARSS)*. IEEE, 2016, pp. 104–107.

[32] Bariscan Yonel, Eric Mason, and Birsen Yazıcı, "Deep learning for passive synthetic aperture radar," *IEEE Journal of Selected Topics in Signal Processing*, vol. 12, no. 1, pp. 90–103, 2017.

[33] Sean Thammakhoune and Emre Yavuz, "Deep learning methods for image reconstruction from angularly sparse data for ct and sar imaging," in *Algorithms for Synthetic Aperture Radar Imagery XXVII*. International Society for Optics and Photonics, 2020, vol. 11393, p. 1139306.

[34] Dung N Tran, Trac D Tran, and Lam Nguyen, "Generative adversarial networks for recovering missing spectral information," in *2018 IEEE Radar Conference (RadarConf18)*. IEEE, 2018, pp. 1223–1227.

[35] Lam Nguyen, Dung N Tran, and Trac D Tran, "Spectral gaps extrapolation for stepped-frequency sar via generative adversarial networks," in *2019 IEEE Radar Conference (RadarConf)*. IEEE, 2019, pp. 1–6.

[36] Ian Goodfellow, Jean Pouget-Abadie, Mehdi Mirza, Bing Xu, David Warde-Farley, Sherjil Ozair, Aaron Courville, and Yoshua Bengio, "Generative adversarial nets," in *Advances in Neural Information Processing Systems*, 2014, pp. 2672–2680.

[37] Sergey Ioffe and Christian Szegedy, "Batch normalization: Accelerating deep network training by reducing internal covariate shift," *arXiv preprint arXiv:1502.03167*, 2015.

[38] Augustus Odena, Vincent Dumoulin, and Chris Olah, "Deconvolution and checkerboard artifacts," *Distill*, vol. 1, no. 10, pp. e3, 2016.

[39] Wenzhe Shi, Jose Caballero, Ferenc Huszár, Johannes Totz, Andrew P Aitken, Rob Bishop, Daniel Rueckert, and Zehan Wang, "Real-time single image and video super-resolution using an efficient sub-pixel convolutional neural network," in *Proceedings of the IEEE Conference on Computer Vision and Pattern Recognition*, 2016, pp. 1874–1883.

[40] Diederik P Kingma and Jimmy Ba, "Adam: A method for stochastic optimization," *arXiv preprint arXiv:1412.6980*, 2014.

[41] Joel A Tropp and Anna C Gilbert, "Signal recovery from random measurements via orthogonal matching pursuit," *IEEE Transactions on Information Theory*, vol. 53, no. 12, pp. 4655–4666, 2007.

[42] Balakrishnan Varadarajan, Sanjeev Khudanpur, and Trac D. Tran, "Stepwise optimal subspace pursuit for improving sparse recovery," *IEEE Signal Processing Letters*, vol. 18, no. 1, pp. 27–30, 2011.